Pergamon

J. Quant. Spectrosc. Radiat. Transfer Vol. 56, No. 3, pp. 337–351, 1996
Published by Elsevier Science Ltd. Printed in Great Britain
0022-4073/96 $15.00 + 0.00

PII: S0022-4073(96)00100-8

BENCHMARK RESULTS FOR THE NON-EQUILIBRIUM MARSHAK DIFFUSION PROBLEM

BINGJING SU† and GORDON L. OLSON

Applied Theoretical and Computational Physics Division, Los Alamos National Laboratory, Los Alamos, NM 87545, U.S.A.

(Received 16 February 1996)

Abstract—As an extension of previous work in the literature, this paper considers a particular one-dimensional, halfspace, non-equilibrium Marshak wave problem. The radiative transfer model employed is a one-group diffusion approximation with Marshak boundary condition, where the radiation and material fields are out of equilibrium. An analytic solution for the distribution of radiative energy and material temperature as a function of space and time to this problem is given and tables of numerical results are generated. These benchmark results, together with the previously published results, are useful as a reference for validating time-dependent radiation diffusion computer codes. A comparison with a finite difference solution is presented which shows excellent agreement when a fine spatial mesh and small time steps are used. Copyright © 1996 Published by Elsevier Science Ltd

1. INTRODUCTION

Due to the complexity of the equation of radiative transfer, the need to include the material energy balance equation, and the generally complex dependence of the material properties on the relevant independent variables, almost all realistic time-dependent radiative transfer problems must be solved numerically. Many computer codes for this type of problem exist in the engineering and scientific community. However, to verify the numerical schemes used in the codes and to test the accuracy and the sensitivity to changes in mesh size (in space and time) of the codes, it is desirable to have benchmark results by analytic methods for some reference problems. Such benchmark results (analytic solutions) for time-dependent radiative transfer reference problems are rare in the literature.

One semi-analytic solution to a time-dependent radiative transfer problem was derived by Marshak.[1] The problem Marshak treated has since been called the Marshak wave problem and corresponds to an initially cold halfspace of material with radiation incident upon the surface. In his treatment, Marshak assumed that the material and radiation fields are in equilibrium, i.e., the radiation field at any time and space point is simply the Planckian at the local material temperature. Under this assumption, the equation of transfer is eliminated, and the problem admits a similarity solution to a second order nonlinear ordinary differential equation, that can be solved numerically.[2] Hence, Marshak's semi-analytic solution is only valid for the equilibrium Marshak diffusion problem.

Pomraning considered the non-equilibrium Marshak diffusion problem with a one group diffusion description,[3] allowing radiation and material fields to develop separately according to the physics of the problem. In order to make the problem tractable analytically, Pomraning introduced a specific dependence of the material heat capacity on the material temperature; he assumed that this heat capacity is proportional to the cube of the temperature. With this assumption, both the equation of transfer and the energy balance equation become linear in radiative energy and the fourth power of the material temperature. As pointed out by Pomraning,[3] the sole purpose of this

†To whom all correspondence should be addressed at: XTM, MS B283, Los Alamos National Laboratory, Los Alamos, NM 87545, U.S.A. or faxed to (565) 655-3003.

assumption is to relax the physical content of the problem such that a detailed analytic solution can be obtained and thus provide a useful test problem for radiative transfer codes, since those codes are meant to handle an arbitrary temperature dependence of the heat capacity. By using the Laplace transform, Pomraning derived the analytic solutions for the surface quantities, integral quantities, and the distributions of radiative energy and material temperature as functions of space and time for the case of the "no retardation" approximation, in which the speed of light is treated as an infinity in the equation of transfer. However, for a more general case where the speed of light is treated as a finite constant, Pomraning only derived the solutions for the spatially integrated radiation and material energies in the slab as functions of time.[3] No solutions or benchmark results were given for the spatial distributions of radiative energy and material temperature. Since such distribution results are essential to fully validate time-dependent radiative transfer computer codes, the purpose of this paper is to extend the work of Pomraning[3] to derive an analytic solution to the problem and generate benchmark results for the distribution of radiative energy and material temperature as a function of space and time when the speed of light is treated as a finite constant in the equation of transfer. The remainder of this paper is organized as follows. The derivation of the analytic solution is given in Sec. 2. The numerical scheme of evaluating the analytic solution and the benchmark numerical results are presented in Sec. 3. These generated benchmark results are compared with a finite difference solution in Sec. 4. Section 5 presents a few concluding remarks.

Before closing this Introduction, we remind our readers that there are two other papers devoted to the derivation of analytic solution to this non-equilibrium Marshak wave problem. Pomraning and Shokair[4] reported a spherical harmonic (P-2) treatment to the problem, and Ganapol and Pomraning[5] considered the problem strictly in a transport description. In both treatments, analytic solutions for the surface and integral quantities were derived. Like the diffusion case, no solutions or benchmark results for the distribution of radiative energy and material temperature as a function of space and time were given. We plan to explore the possibility of providing this missing but definitely desirable information for the transport description in the near future and will report any positive progress in a future publication. However, the full transport solution is considerably more difficult to derive and to evaluate numerically than the diffusion solution presented here.

2. ANALYSIS

We consider the same non-equilibrium Marshak wave problem as Pomraning.[3] For completeness and clarity of the presentation, a portion of the analysis in Ref. 3 is reproduced in this section. The non-equilibrium Marshak wave problem consists of a semi-infinite, purely absorbing, and homogeneous medium occupying $0 \leqslant z < \infty$. The medium is at a zero temperature with no radiation field present at time $t < 0$. Commencing at $t = 0$, a time independent radiative flux impinges upon the surface at $z = 0$. Neglecting hydrodynamic motion and heat conduction, the one group radiative transfer equation in the diffusion approximation and the material energy balance equation are[3]

$$\frac{\partial E(z, t)}{\partial t} - \frac{\partial}{\partial z}\left[\frac{c}{3\kappa(T)}\frac{\partial E(z, t)}{\partial z}\right] = c\kappa(T)[aT^4(z, t) - E(z, t)], \tag{1}$$

$$c_v(T)\frac{\partial T(z, t)}{\partial t} = c\kappa(T)[E(z, t) - aT^4(z, t)], \tag{2}$$

where $E(z, t)$ is the radiation energy density, $T(z, t)$ is the material temperature, $\kappa(T)$ is the absorption cross section (opacity), c is the speed of light, a is the radiation constant, and $c_v(T)$ is the heat capacity of the material. The Marshak boundary condition on Eq. (1) at $z = 0$ is given by

$$E(0, t) - \left(\frac{2}{3\kappa[T(0, t)]}\right)\frac{\partial E(0, t)}{\partial z} = \frac{4}{c}F_{\text{inc}}, \tag{3}$$

where F_{inc} is the flux incident upon the surface $z = 0$. The boundary condition at $z = \infty$ on Eq. (1) is

$$E(\infty, t) = 0, \tag{4}$$

and the initial conditions on these two equations are

$$E(z, 0) = T(z, 0) = 0. \tag{5}$$

Equations (1) and (2), together with the boundary and initial conditions, Eqs. (3)–(5), define the two unknowns that we wish to compute, namely, $E(z, t)$ and $T(z, t)$. Equations (1) and (2) are clearly nonlinear for a general temperature dependence of $\kappa(T)$ and $c_v(T)$. To remove this nonlinearity, Pomraning[3] assumed that κ is independent of temperature, and c_v is proportional to the cube of the temperature, i.e.,

$$c_v = \alpha T^3. \tag{6}$$

Then Eqs. (1) and (2) become linear in E and T^4. Further, Pomraning[3] recast these equations into dimensionless form by introducing the dimensionless independent variables given by

$$x \equiv \sqrt{3}\kappa z, \quad \tau \equiv \left(\frac{4ac\kappa}{\alpha}\right)t, \tag{7}$$

and new dependent variables given by

$$u(x, \tau) \equiv \left(\frac{c}{4}\right)\left[\frac{E(z, t)}{F_{inc}}\right], \quad v(x, \tau) \equiv \left(\frac{c}{4}\right)\left[\frac{aT^4(z, t)}{F_{inc}}\right]. \tag{8}$$

With these new variables, Eqs. (1)–(5) take the dimensionless form

$$\epsilon\frac{\partial u(x, \tau)}{\partial \tau} - \frac{\partial^2 u(x, \tau)}{\partial x^2} = v(x, \tau) - u(x, \tau), \tag{9}$$

$$\frac{\partial v(x, \tau)}{\partial \tau} = u(x, \tau) - v(x, \tau), \tag{10}$$

$$u(0, \tau) - \frac{2}{\sqrt{3}}\frac{\partial u(0, \tau)}{\partial x} = 1, \tag{11}$$

$$u(\infty, \tau) = u(x, 0) = v(x, 0) = 0, \tag{12}$$

where the parameter ϵ is defined as

$$\epsilon = \frac{16\sigma}{c\alpha} = \frac{4a}{\alpha}. \tag{13}$$

Here σ in Eq. (13) is the Stefan–Boltzmann constant and is given by $\sigma = ac/4$.

To solve Eqs. (9)–(12), we introduce the Laplace transform according to

$$\bar{f}(s) = \int_0^\infty d\tau\, e^{-s\tau} f(\tau) \tag{14}$$

to Eqs. (9)–(12) and obtain

$$\epsilon s\bar{u}(x, s) - \frac{\partial^2 \bar{u}(x, s)}{\partial x^2} = \bar{v}(x, s) - \bar{u}(x, s), \tag{15}$$

$$s\bar{v}(x, s) = \bar{u}(x, s) - \bar{v}(x, s), \tag{16}$$

$$\bar{u}(0, s) - \frac{2}{\sqrt{3}}\frac{\partial \bar{u}(0, s)}{\partial x} = \frac{1}{s}, \tag{17}$$

$$\bar{u}(\infty, s) = 0. \tag{18}$$

Equations (15)–(18) yield the following solutions,[3] in s space,

$$\bar{u}(x, s) = \frac{\sqrt{3}\, e^{-\beta(s)x}}{s[\sqrt{3} + 2\beta(s)]}, \tag{19}$$

$$\bar{v}(x, s) = \frac{\sqrt{3}\, e^{-\beta(s)x}}{s(s+1)[\sqrt{3} + 2\beta(s)]}, \tag{20}$$

where $\beta(s)$ is given by

$$\beta^2(s) = \left(\frac{s}{s+1}\right)[1 + \epsilon(s+1)]. \tag{21}$$

The solutions for $u(x, \tau)$ and $v(x, \tau)$ follow Eqs. (19) and (20) by the Laplace inverse transform. In Ref. 3, Pomraning considered the case "$\epsilon = 0$" carefully and derived analytic solutions for the surface quantities $u(0, \tau)$ and $v(0, \tau)$, the integral quantities $\psi_r(\tau)$ and $\psi_m(\tau)$, which are defined as

$$\psi_r(\tau) = \int_0^\infty dx u(x, \tau), \quad \psi_m(\tau) = \int_0^\infty dx v(x, \tau), \tag{22}$$

and the distributions $u(x, \tau)$ and $v(x, \tau)$ as functions of space and time. Detailed benchmark results were given for this special case.[3] As mentioned previously, setting the parameter ϵ to zero corresponds to the "no retardation" approximation, which implies that, as far as the radiative transfer process is concerned, the speed of light is infinite [see Eq. (1)], and that the radiation field instantly comes into a steady-state distribution with the material temperature distribution at any time. However, for the general case of an arbitrary ϵ, Pomraning only gave the analytic solutions for the $\psi_r(\tau)$ and $\psi_m(\tau)$, not for $u(x, \tau)$ and $v(x, \tau)$. Since these distribution results, $u(x, \tau)$ and $v(x, \tau)$, as well as $\psi_r(\tau)$ and $\psi_m(\tau)$, for an arbitrary ϵ are required for validating time-dependent radiative transfer computer codes (in the diffusion approximation), we will focus on deriving the analytic solutions and generating benchmark results for $u(x, \tau)$ and $v(x, \tau)$ with an arbitrary ϵ.

We now invert $\bar{u}(x, s)$ back to $u(x, \tau)$, with ϵ arbitrary, by the Laplace inversion theorem

$$f(\tau) = \frac{1}{2\pi i}\int_C ds\, e^{s\tau}\bar{f}(s), \tag{23}$$

where the integration contour C is a line parallel to the imaginary s axis to the right of all the singularities of $\bar{f}(s)$. Using $\beta(s)$ in Eq. (19), we have

$$\bar{u}(x, s) = \frac{\sqrt{3(s+1)}\exp[-x\sqrt{s}\sqrt{\epsilon + 1/(s+1)}]}{s[\sqrt{3(s+1)} + 2\sqrt{s}\sqrt{1 + \epsilon(s+1)}]}. \tag{24}$$

Clearly, the singularities of $\bar{u}(x, s)$ include branch points at $s = 0$, $s = -1$, and $s = -(1 + 1/\epsilon)$. We define the proper branches as those which give a positive square root for s lying on the real positive axis and extend all three branch cuts along the negative real axis. The function $\bar{u}(x, s)$ also has a simple pole at $s = 0$ and two simple poles at

$$s = -\left(\frac{1}{8\epsilon}\right)[1 + 4\epsilon \pm \sqrt{1 + 56\epsilon + 16\epsilon^2}]. \tag{25}$$

However, the poles given by Eq. (25) are on the nonphysical Riemann sheet[3] and hence can be ignored. To find out the solution for $u(x, \tau)$, we consider a closed integration contour shown in Fig. 1, and the integrand under consideration is just the product of the $\bar{u}(x, s)$ given by Eq. (24) and $e^{s\tau}$. Since the integrand has no singularity within the closed contour, we have

$$I_C + I_R + I_r + I_P + I_N = 0, \tag{26}$$

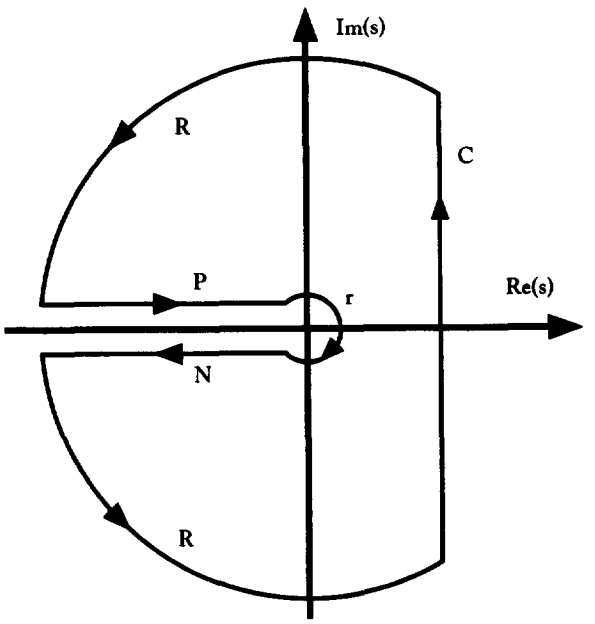

Fig. 1. The integration contour for the Laplace inverse transform.

where I_l represents the integral on the contour l. It can be proved that the integration on the large semicircle contour R gives a zero contribution as usual, as $|s|$ goes to ∞, i.e.,

$$I_R = 0. \tag{27}$$

According to the residue theorem, the integral on the small circle r, as $|s|$ goes to zero, is simply equal to the product of $(-2\pi i)$ and its residue at $s = 0$, thus we have

$$I_r = -2\pi i. \tag{28}$$

Then from Eq. (26), we deduce that the integral we are interested in, I_C, is given by

$$I_C = 2\pi i - (I_P + I_N), \tag{29}$$

and in turn the $u(x, \tau)$ is expressed as, according to Eq. (23),

$$u(x, \tau) = \frac{1}{2\pi i} I_C = 1 - \frac{1}{2\pi i}(I_P + I_N). \tag{30}$$

It is relatively easy to calculate I_P and I_N, since on these contours we have $s = -\xi$, where ξ is real and positive. Note that I_P and I_N do not necessarily cancel each other, because on the contour P we have $\sqrt{s} = i\sqrt{\xi}$ while on the contour N we have $\sqrt{s} = -i\sqrt{\xi}$ so that the $\bar{u}(x, s)$ is different on these two integration contours. Specifically in our case, we find cancellation between I_P and I_N on the interval $-(1 + 1/\epsilon) \leqslant s \leqslant -1$, but not on the intervals $-\infty < s \leqslant -(1 + 1/\epsilon)$ and $-1 \leqslant s \leqslant 0$.

Omitting the algebraic detail of manipulating I_P and I_N, we obtain

$$u(x, \tau) = 1 - \frac{\sqrt{3}}{\pi} \int_0^{1} d\xi \, e^{-\xi\tau} \left[\frac{2\gamma \cos(x\gamma) + \sqrt{3} \sin(x\gamma)}{\xi(3 + 4\gamma^2)} \right]$$

$$- \frac{\sqrt{3}}{\pi} \int_{(1 + 1/\epsilon)}^{\infty} d\xi \, e^{-\xi\tau} \left[\frac{2\gamma \cos(x\gamma) + \sqrt{3} \sin(x\gamma)}{\xi(3 + 4\gamma^2)} \right], \tag{31}$$

where γ is defined as

$$\gamma(\xi) = \sqrt{\frac{\xi|1+\epsilon-\epsilon\xi|}{|1-\xi|}} = \begin{cases} \sqrt{\dfrac{\xi(1+\epsilon-\epsilon\xi)}{1-\xi}}, & 0<\xi<1, \\ \sqrt{\dfrac{\xi(\epsilon\xi-1-\epsilon)}{\xi-1}}, & (1+1/\epsilon)<\xi<\infty \end{cases} . \tag{32}$$

We can simplify the expression of $u(x,\tau)$ by defining

$$\theta(\xi) = \cos^{-1}\sqrt{\frac{3}{3+4\gamma^2(\xi)}}, \tag{33}$$

then Eq. (31) can be rewritten as

$$u(x,\tau) = 1 - \frac{\sqrt{3}}{\pi}\int_0^1 d\xi\, e^{-\xi\tau}\left[\frac{\sin[x\gamma(\xi)+\theta(\xi)]}{\xi\sqrt{3+4\gamma^2(\xi)}}\right] - \frac{\sqrt{3}}{\pi}\int_{(1+1/\epsilon)}^{\infty} d\xi\, e^{-\xi\tau}\left[\frac{\sin[x\gamma(\xi)+\theta(\xi)]}{\xi\sqrt{3+4\gamma^2(\xi)}}\right]. \tag{34}$$

This expression must be evaluated numerically. The integrand of the first integral in Eq. (34) has an integrable singularity at $\xi = 0$. Because as $\xi \to 0$, we have $\gamma \to \sqrt{\xi(1+\epsilon)}$, which in turn reduces the integrand to $x\sqrt{(1+\epsilon)/(3\xi)}$. To remove this singularity at $\xi = 0$, we change integration variables according to $\xi = \eta^2$ as was done earlier[3] in the first integral. The integrand of the second integral in Eq. (34) has no singularity on the integration interval. However, we like to have a finite integration interval so we change the integration variables according to

$$\xi - 1 = \frac{1}{\epsilon\eta} \tag{35}$$

in the second integral. After these changes, Eq. (34) becomes

$$u(x,\tau) = 1 - \frac{2\sqrt{3}}{\pi}\int_0^1 d\eta\, e^{-\tau\eta^2}\left[\frac{\sin[x\gamma_1(\eta)+\theta_1(\eta)]}{\eta\sqrt{3+4\gamma_1^2(\eta)}}\right]$$

$$- \frac{\sqrt{3}}{\pi}e^{-\tau}\int_0^1 d\eta\, e^{-\tau/(\epsilon\eta)}\left[\frac{\sin[x\gamma_2(\eta)+\theta_2(\eta)]}{\eta(1+\epsilon\eta)\sqrt{3+4\gamma_2^2(\eta)}}\right], \tag{36}$$

where

$$\gamma_1(\eta) = \eta\sqrt{\epsilon + \frac{1}{(1-\eta^2)}}, \quad \gamma_2(\eta) = \sqrt{(1-\eta)\left(\epsilon+\frac{1}{\eta}\right)}, \tag{37}$$

and

$$\theta_n(\eta) = \cos^{-1}\sqrt{\frac{3}{3+4\gamma_n^2(\eta)}}, \quad n = 1, 2. \tag{38}$$

Equation (36) is the final expression we will use to compute $u(x,\tau)$. The integrands in Eq. (36) have no singularity. As $\eta \to 0$, we have $\gamma_1 \to \eta\sqrt{1+\epsilon}$, that reduces the first integrand to $(2/3 + x/\sqrt{3})\sqrt{1+\epsilon}$, which is finite. And obviously, the second integrand is zero at $\eta = 0$ because of the exponential term.

Once the $u(x,\tau)$ is obtained, we have two ways to derive the solution for $v(x,\tau)$. The first method is based on Eq. (10), from which we deduce that

$$v(x,\tau) = \int_0^\tau d\tau'\, e^{-(\tau-\tau')}u(x,\tau'). \tag{39}$$

One could obtain the $v(x, \tau)$ by using the $u(x, \tau)$ in Eq. (39). The second way is to apply the same inversion procedure (including the closed integration contour shown in Fig. 1) for the $\bar{u}(x, s)$ to the $\bar{v}(x, s)$ and thus find the solution for $v(x, \tau)$. We omit the algebraic detail and simply give the result

$$v(x,\tau) = 1 - \frac{\sqrt{3}}{\pi}\int_0^1 d\xi\, e^{-\xi\tau}\left[\frac{\sin[x\gamma(\xi)+\theta(\xi)]}{\xi(1-\xi)\sqrt{3+4\gamma^2(\xi)}}\right] - \frac{\sqrt{3}}{\pi}\int_{(1+1/c)}^{\infty} d\xi\, e^{-\xi\tau}\left[\frac{\sin[x\gamma(\xi)+\theta(\xi)]}{\xi(1-\xi)\sqrt{3+4\gamma^2(\xi)}}\right], \tag{40}$$

with γ and θ defined by Eqs. (32) and (33). Equation (40) can be rewritten as

$$v(x,\tau) = u(x,\tau) - \frac{\sqrt{3}}{\pi}\int_0^1 d\xi\, e^{-\xi\tau}\left[\frac{\sin[x\gamma(\xi)+\theta(\xi)]}{(1-\xi)\sqrt{3+4\gamma^2(\xi)}}\right] - \frac{\sqrt{3}}{\pi}\int_{(1+1/c)}^{\infty} d\xi\, e^{-\xi\tau}\left[\frac{\sin[x\gamma(\xi)+\theta(\xi)]}{(1-\xi)\sqrt{3+4\gamma^2(\xi)}}\right]. \tag{41}$$

For the same reasons as in the case of $u(x, \tau)$, we change integration variables in Eq. (41). For the first integral, we change variables according to $1 - \xi = \eta^2$; and for the second integral, we change variables according to Eq. (35) again. These changes yield

$$v(x,\tau) = u(x,\tau) - \frac{2\sqrt{3}}{\pi}\int_0^1 d\eta\, e^{-\tau(1-\eta^2)}\left[\frac{\sin[x\gamma_3(\eta)+\theta_3(\eta)]}{\sqrt{4-\eta^2+4\epsilon\eta^2(1-\eta^2)}}\right] + \frac{\sqrt{3}}{\pi}e^{-\tau}\int_0^1 d\eta\, e^{-\tau/(c\eta)}\left[\frac{\sin[x\gamma_2(\eta)+\theta_2(\eta)]}{\eta\sqrt{3+4\gamma_2^2(\eta)}}\right], \tag{42}$$

where

$$\gamma_3(\eta) = \sqrt{(1-\eta^2)\left(\epsilon+\frac{1}{\eta^2}\right)}, \quad \theta_3(\eta) = \cos^{-1}\sqrt{\frac{3}{3+4\gamma_3^2(\eta)}}. \tag{43}$$

Equations (36) and (42) are the solutions for $u(x, \tau)$ and $v(x, \tau)$ for the general case of an arbitrary ϵ. When setting $\epsilon = 0$, we can easily see that the second integrals in Eqs. (36) and (42) vanish, and verify that the remaining parts reduce to the solutions obtained by Pomraning[3] for the case of $\epsilon = 0$. [By the way, the solution for $u(x, \tau)$ given in Ref. 3, i.e., Eq. (75) on p. 258, has a typographical error: the denominator of the coefficient in the second integral should be $\eta(3 + \eta^2)$ instead of the $(3 + \eta^2)$ given in the paper.] Further, when substituting Eqs. (36) and (42) in Eqs. (9)–(11), we can verify that the $u(x, \tau)$ and $v(x, \tau)$ derived in this section satisfy the governing equations and the boundary condition. These checks give us confidence in our treatment and algebraic manipulations.

3. NUMERICAL BENCHMARK RESULTS

In this section, we present the benchmark results for the $u(x, \tau)$ and $v(x, \tau)$, computed according to Eqs. (36) and (42). The integrals in these two equations are evaluated numerically. Because of the oscillations of the trigonometric functions in the integrands, the whole integration range $(0 \leqslant \eta \leqslant 1)$ is divided into several subranges for each integral. We consider a little bit in detail the first integral in Eq. (36), whose integrand contains $\sin(x\gamma_1)$ and $\cos(x\gamma_1)$ if the $\sin(x\gamma_1 + \theta_1)$ is expanded explicitly. As the integration variable η goes from 0 to 1, the quantity γ_1, as a function of η, changes from 0 to ∞ [see Eq. (37)]. This implies that $x\gamma_1$ experiences an infinite number of

2π cycles, assuming that $x \neq 0$. It is easy to find the points η_j, which correspond to $x\gamma_1$ being equal to $j2\pi$, by solving

$$\gamma_1(\eta_j) \equiv \eta_j \sqrt{\epsilon + \frac{1}{(1-\eta_j^2)}} = \frac{j2\pi}{x}, \quad j = 1, 2, \ldots, m. \tag{44}$$

The trigonometric functions $\sin(x\gamma_1)$ and $\cos(x\gamma_1)$ experience a complete period when η changes from η_{j-1} to η_j, thus we define $\eta_{j-1} \leqslant \eta \leqslant \eta_j$ (with $\eta_0 = 0$) as the jth ($j = 1, 2, \ldots, m$) integration subrange. We arbitrarily set the last, or the $(m+1)$th, subrange to cover $\eta_m \leqslant \eta \leqslant 1$. For each subrange, including the last one, the integral is evaluated by Simpson's rule,[6] i.e., the integration subrange $\eta_{j-1} \leqslant \eta \leqslant \eta_j$ is divided into 2^N equal intervals and N is successively increased from $N = 1, 2, 3, \ldots$ until a desired accuracy is achieved. We require the numerical results of $u(x, \tau)$ and $v(x, \tau)$ to have five digits after the decimal point; therefore, the convergence criteria is set to be 0.001%. Specifically, the integral for each subrange is thought to be converged when a relative error of 0.001% is achieved between two successive numerical evaluations (with halved intervals). The value of m (corresponding to the number of subranges) is determined in such a way that the mth subrange is the first cycle in which the absolute value of the integral under consideration is less than 1×10^{-6}. This value (1×10^{-6}) is selected so that the last integration subrange, which still covers infinite 2π cycles for $x\gamma_1$ and thus makes the integral hard to converge, contributes little or nothing to the total integration within the accuracy requirement. In order to avoid unnecessary computation for the last subrange, we set a check point in the convergence process. If the absolute value of the integral in this subrange, after convergence to 0.1% relative accuracy, is found to be less than 1×10^{-5}, then there is no need to continue to converge this value to a higher accuracy and the convergence process is stopped.

The same procedure is also applied to the other three integrals, which involve $x\gamma_2$ and $x\gamma_3$. The only difference, compared with the case of $x\gamma_1$, is that when η goes from 0 to ∞, γ_2 and γ_3 both change from ∞ to 0. Hence, solving equations similar to Eq. (44) for γ_2 and γ_3, we find $\eta_j < \eta_{j-1}$. This means that the first 2π cycle for $\sin(x\gamma_2)$ or $\sin(x\gamma_3)$ appears near $\eta = 1$, contrary to the case of $\sin(x\gamma_1)$. Thus, we define the jth ($j = 1, 2, \ldots, m$) integration subrange as $\eta_j \leqslant \eta \leqslant \eta_{j-1}$ (with $\eta_0 = 1$) accordingly, and set the last subrange to cover $0 \leqslant \eta \leqslant \eta_m$.

To test the analytic solution and particularly the numerical scheme just outlined, we compared our numerical results with the "known" solutions for some special cases. We first consider the τ limits of $u(x, \tau)$ and $v(x, \tau)$. Based on Eqs. (19) and (20), and using the theorems

$$\lim_{s\to\infty} [s\bar{f}(s)] = \lim_{\tau\to 0} [f(\tau)], \tag{45}$$

$$\lim_{s\to 0} [s\bar{f}(s)] = \lim_{\tau\to\infty} [f(\tau)], \tag{46}$$

we easily have

$$u(x, 0) = v(x, 0) = 0, \tag{47}$$

$$u(x, \tau) \underset{\tau\to\infty}{\to} v(x, \tau) \underset{\tau\to\infty}{\to} 1. \tag{48}$$

Equation (47) is simply the initial conditions [see Eq. (12)]. Equation (48) states that at infinite time, both the radiation and material temperature approach the same constant, which is unity in our dimensionless form. Although we cannot simulate the $\tau \to \infty$ solution, the results at $\tau = 0$ are very good references for our test. Using our analytic solution and the numerical procedure, we obtained $u(0, 0) = 0.00001$ and $v(0, 0) = 0.00000$ for $\epsilon = 0.1$, and $u(1, 0) = -0.00001$ and $v(1, 0) = 0.00000$ for $\epsilon = 1.0$. Compared with Eq. (47), these results shows that our algorithm predicts the correct values for this case and that the benchmark results generated in such a way have absolute errors of the order of 10^{-5}. The latter point is obvious. The integrals, computed according to our numerical scheme, have relative errors of 0.001%, and the sum of the integrals in Eq. (36) is of the order of 1 at small τ, like the case of $\tau = 0$ we are considering. This implies that the absolute errors of the numerical integrations are in the order of 10^{-5} for small τ. Thus, the numerical results for $u(x, \tau)$ and $v(x, \tau)$ have absolute errors of order 10^{-5} in general and accordingly they are given only the first five digits after the decimal point. However, as τ increases, the contribution of the

integrals tends to decrease (much less than unity for large τ). Thus, the absolute errors of the results at large τ are expected to be less than that at small τ.

Next, we consider a boundary layer solution in the time variable at $x = 0$, which shows rapidly varying time behavior for small τ. As $s \to \infty$, $\bar{u}(0, s)$ and $\bar{v}(0, s)$ reduce to [see Eqs. (19) and (20)]

$$\bar{u}(0, s) \underset{s\to\infty}{\to} \frac{\sqrt{3}}{2\sqrt{\epsilon s^{3/2}}} - \frac{3}{4\epsilon s^2} + \frac{\sqrt{3}}{8\epsilon^{3/2} s^{5/2}} + O\left(\frac{1}{s^3}\right), \tag{49}$$

$$\bar{v}(0, s) \underset{s\to\infty}{\to} \frac{\sqrt{3}}{2\sqrt{\epsilon s^{5/2}}} + O\left(\frac{1}{s^3}\right). \tag{50}$$

Converting Eqs. (49) and (50) back to the τ space, we have

$$u(0, \tau) = \sqrt{\frac{3\tau}{\pi\epsilon}} - \frac{3\tau}{4\epsilon} + \frac{\tau}{2\epsilon}\sqrt{\frac{\tau}{3\pi\epsilon}} + O(\tau^2), \tag{51}$$

$$v(0, \tau) = 2\tau\sqrt{\frac{\tau}{3\pi\epsilon}} + O(\tau^2). \tag{52}$$

Equations (51) and (52) are the asymptotic boundary layer solutions (in the time variable) for $u(0, \tau)$ and $v(0, \tau)$, and are only valid for small τ, with absolute errors in the order of τ^2. Therefore, for very small τ (say $\tau < 1 \times 10^{-3}$) and $x = 0$, the fully analytic solution given by Eqs. (36) and (42), valid for any x and any τ, and the asymptotic boundary layer solution given by Eqs. (51) and (52), valid only for $x = 0$ and small τ, should predict practically the same results. To check this boundary layer behavior, we calculated $u(0, \tau)$ and $v(0, \tau)$ for $\tau = 1 \times 10^{-4}$ and $\epsilon = 0.1$ with our numerical procedure and obtained $u = 0.03016$ and $v = 0.00000$ while Eqs. (51) and (52) predict $u = 0.030157$ and $v = 2.060 \times 10^{-6}$. And for $\tau = 5 \times 10^{-3}$ and $\epsilon = 1.0$, the analytic solution yielded $u = 0.06541$ and $v = 0.00023$, with the asymptotic solution predicting $u = 0.065406$ and $v = 2.303 \times 10^{-4}$. We see that the two solutions agree with each other exactly for the first five digits after the decimal point, as they should. Certainly, as the increase of τ, the asymptotic solution become less accurate and thus the agreement between the asymptotic solution and the analytic solution deteriorates. These preliminary comparisons validate the analytic solutions and particularly the numerical scheme employed at least to some extent.

Using the foregoing algorithm, we computed benchmark results of $u(x, \tau)$ and $v(x, \tau)$ for $\epsilon = 0.1$ and $\epsilon = 1.0$, and list these results in Tables 1–4, respectively. The values given in the tables are believed to be accurate at least to the first four digits after the decimal point, for the reason stated earlier. Even though we broke up the integration range into $m + 1$ subranges, the oscillation of the trigonometric functions in the integrands still makes the numerical integration in a subrange not easy to converge when the contribution from that subrange is very small (say less than 10^{-4}). With a convergence criteria of 0.001%, the integration subranges usually need to be divided into 2^5–2^{15} equal intervals for the integrals to converge for the first m cycles. And the number of intervals in the last subrange, which includes infinite 2π cycles, may have to go beyond 2^{20} for the integral to converge to the required accuracy. However, this slow convergence does not pose a serious difficulty to the computation, thanks to the advance of computer technology. The computation of the integrals for a few extreme hard cases could be done in an hour when using a modern personal computer or workstation; while for the other cases, the computation only took seconds or minutes.

4. FINITE DIFFERENCE SOLUTION

This section will present a finite difference solution to the differential equations defined in Sec. 2 and compare this solution to the analytic solution presented in Sec. 3. In order to make the

Table 1. The benchmark results of $u(x, \tau)$ for $\epsilon = 0.1$.

τ \ x	0	0.1	0.25	0.5	0.75	1	2.5	5	7.5	10	15	20
0.001	0.09039	0.03241	0.00360	0.00001								
0.003	0.14768	0.08521	0.03042	0.00293	0.00012							
0.01	0.23997	0.17979	0.11006	0.04104	0.01214	0.00268						
0.03	0.34328	0.28962	0.22063	0.13345	0.07545	0.03958	0.00014					
0.1	0.43876	0.39240	0.33075	0.24629	0.18087	0.13089	0.01274	0.00005				
0.3	0.48556	0.44289	0.38544	0.30500	0.24062	0.18922	0.04167	0.00238	0.00008			
1	0.55182	0.51412	0.46198	0.38541	0.32046	0.26564	0.08147	0.00961	0.00097	0.00009		
3	0.66334	0.63458	0.59295	0.52771	0.46773	0.41298	0.18266	0.03844	0.00678	0.00105	0.00003	
10	0.79420	0.77644	0.75004	0.70679	0.66458	0.62353	0.40703	0.17142	0.06123	0.01909	0.00135	0.00007
30	0.87731	0.86669	0.85082	0.82451	0.79839	0.77252	0.62363	0.40954	0.24817	0.13893	0.03473	0.00660
100	0.93202	0.92613	0.91731	0.90263	0.88799	0.87338	0.78683	0.64880	0.52202	0.40952	0.23303	0.11915

Table 2. The benchmark results of $v(x, \tau)$ for $\epsilon = 0.1$.

τ \ x	0	0.1	0.25	0.5	0.75	1	2.5	5	7.5	10	15	20
0.001	0.00006	0.00002										
0.003	0.00030	0.00014	0.00004									
0.01	0.00170	0.00110	0.00055	0.00012	0.00003							
0.03	0.00762	0.00592	0.00398	0.00196	0.00088	0.00027						
0.1	0.03446	0.02955	0.02339	0.01566	0.01030	0.00672	0.00035	0.00001				
0.3	0.11322	0.10124	0.08551	0.06437	0.04830	0.03612	0.00584	0.00020	0.00001			
1	0.32030	0.29429	0.25915	0.20925	0.16862	0.13563	0.03539	0.00334	0.00028	0.00003		
3	0.58906	0.55843	0.51488	0.44845	0.38930	0.33690	0.13377	0.02432	0.00381	0.00054	0.00002	
10	0.78318	0.76448	0.73673	0.69139	0.64730	0.60461	0.38320	0.15285	0.05166	0.01527	0.00098	0.00005
30	0.87523	0.86443	0.84829	0.82154	0.79500	0.76871	0.61768	0.40167	0.24046	0.13273	0.03213	0.00589
100	0.93167	0.92576	0.91689	0.90214	0.88743	0.87275	0.78578	0.64715	0.51993	0.40717	0.23071	0.11735

QSRT 56/3—B

Table 3. The benchmark results of $u(x, \tau)$ for $\epsilon = 1.0$.

τ \ x	0	0.1	0.25	0.5	0.75	1	2.5	5	7.5	10	15	20
0.001	0.03016	0.00034										
0.003	0.05130	0.00605	0.00003									
0.01	0.09040	0.03241	0.00361	0.00001								
0.03	0.14769	0.08522	0.03043	0.00294	0.00012							
0.1	0.24023	0.18003	0.11024	0.04111	0.01217	0.00280						
0.3	0.34619	0.29261	0.22334	0.13531	0.07653	0.04016	0.00014					
1	0.46599	0.42133	0.36020	0.27323	0.20332	0.14837	0.01441	0.00005	0.00001			
3	0.58965	0.55471	0.50462	0.42762	0.35891	0.29847	0.08222	0.00505	0.00015	0.00001		
10	0.73611	0.71338	0.67978	0.62523	0.57274	0.52255	0.27705	0.07075	0.01271	0.00167	0.00002	
30	0.83793	0.82392	0.80302	0.76849	0.73442	0.70087	0.51363	0.27157	0.12325	0.04803	0.00469	0.00027
100	0.90895	0.90107	0.88926	0.86965	0.85011	0.83067	0.71657	0.54080	0.38982	0.26789	0.10906	0.03624

Table 4. The benchmark results of $v(x, \tau)$ for $\epsilon = 1.0$.

τ \ x	0	0.1	0.25	0.5	0.75	1	2.5	5	7.5	10	15	20
0.001	0.00002											
0.003	0.00010	0.00001										
0.01	0.00062	0.00014	0.00001									
0.03	0.00302	0.00135	0.00034	0.00002								
0.1	0.01641	0.01068	0.00532	0.00143	0.00032	0.00005						
0.3	0.06844	0.05353	0.03639	0.01822	0.00854	0.00367	0.00001					
1	0.24762	0.21614	0.17530	0.12182	0.08306	0.05556	0.00324	0.00001				
3	0.51337	0.47651	0.42483	0.34810	0.28252	0.22719	0.05123	0.00226	0.00005			
10	0.72328	0.69946	0.66432	0.60749	0.55308	0.50134	0.25413	0.05936	0.00968	0.00115	0.00001	
30	0.83529	0.82105	0.79981	0.76474	0.73015	0.69611	0.50660	0.26374	0.11733	0.04465	0.00413	0.00023
100	0.90849	0.90057	0.88871	0.86900	0.84937	0.82983	0.71521	0.53877	0.38745	0.26551	0.10732	0.03534

presentation more coherent, Eqs. (1), (2), and (3) are rewritten as:

$$\frac{\partial E}{\partial t} + \frac{\partial F}{\partial z} = c\kappa(\theta - E), \tag{53}$$

$$F = -\frac{c}{3\kappa}\frac{\partial E}{\partial z}, \tag{54}$$

$$\frac{1}{c}\frac{\partial \theta}{\partial t} = \epsilon\kappa(E - \theta), \tag{55}$$

$$cE(0, t) + 2F(0, t) = 4F_{\text{inc}}, \tag{56}$$

where Pomraning's assumption[3] about the temperature dependence of the heat capacity has been included, the radiation flux, F, has been introduced as an explicit variable, and $\theta \equiv aT^4$ is the material blackbody energy density (not to be confused with the θ used in Sec. 2). All the other variables are the same as in Sec. 2. In the time-dependent P_1 equations, there would be a time derivative of the flux included in Eq. (54). Here we are examining the pure diffusion case without any flux limiting, so that term is dropped and one has a simple Fix's law of diffusion.

First, we perform the time differencing on Eq. (55), using a fully implicit backward Euler scheme:

$$\frac{1}{c}\frac{\partial \theta}{\partial t} = \frac{1}{c\Delta t}(\theta^{n+1} - \theta^n) \equiv \gamma(\theta^{n+1} - \theta^n) = \epsilon\kappa(E^{n+1} - \theta^{n+1}) \tag{57}$$

or:

$$\theta^{n+1} = \frac{\gamma}{\gamma + \epsilon\kappa}\theta^n + \frac{\epsilon\kappa}{\gamma + \epsilon\kappa}E^{n+1}, \tag{58}$$

where the superscript n denotes the time level at which a variable is evaluated. With this definition of γ (not to be confused with a different γ in Sec. 2) as an inverse distance, the time step appears in the equations as an effective opacity. This type of time differencing and an alternative have been discussed by Mihalas and Weaver.[7] Note that the material energy density is a simple linear combustion of the old value and the radiation density at the new time step. Doing a similar time differencing of Eq. (53) and inserting Eq. (58) yields:

$$\frac{1}{c}\frac{\partial E}{\partial t} = \gamma(E^{n+1} - E^n) = -\frac{1}{c}\frac{\partial F^{n+1}}{\partial z} + \kappa(\theta^{n+1} - E^{n+1})$$

$$= -\frac{1}{c}\frac{\partial F^{n+1}}{\partial z} + \kappa\left(\frac{\gamma}{\gamma + \epsilon\kappa}\theta^n + \frac{\epsilon\kappa}{\gamma + \epsilon\kappa}E^{n+1} - E^{n+1}\right), \tag{59}$$

or

$$\left(1 + \frac{\kappa}{\gamma + \epsilon\kappa}\right)\gamma E^{n+1} + \frac{1}{c}\frac{\partial F^{n+1}}{\partial z} = \gamma E^n + \frac{\kappa\gamma}{\gamma + \epsilon\kappa}\theta^n. \tag{60}$$

The spatial discretization will be on a staggered mesh where the independent spatial variable, z, and the flux, F, will be evaluated at cell edges while the energy densities will represent cell averages at the cell centers. Integrating Eq. (60) from $z_{i-1/2}$ to $z_{i+1/2}$ and dividing by $\Delta z_i \equiv z_{i+1/2} - z_{i-1/2}$ gives:

$$\left(1 + \frac{\kappa}{\gamma + \epsilon\kappa}\right)\gamma E_i^{n+1} + \frac{1}{c\Delta z_i}(F_{i+1/2}^{n+1} - F_{i-1/2}^{n+1}) = \gamma E_i^n + \frac{\kappa\gamma}{\gamma + \epsilon\kappa}\theta_i^n. \tag{61}$$

In the problem of interest here, the opacity is constant, but in a more realistic problem, a cell averaged opacity would be used in Eq. (61). There are many ways to discretize the flux in Eq. (54).

Here we shall assume that the energy density is a piecewise linear function in space and define two fluxes at each cell edge, one from the left and one from the right:

$$F_{l,i+1/2}^{n+1} = -\frac{2c}{3\kappa}\frac{(E_{i+1/2}^{n+1} - E_i^{n+1})}{\Delta z_i} \tag{62}$$

$$F_{r,i+1/2}^{n+1} = -\frac{2c}{3\kappa}\frac{(E_{i+1}^{n+1} - E_{i+1/2}^{n+1})}{\Delta z_{i+1}} \tag{63}$$

These two expressions use the cell edge value of the radiation energy density which is unknown. By setting these expressions equal to each other, i.e., requiring that the flux is continuous from one cell to the next, one can solve for this edge energy density:

$$E_{i+1/2}^{n+1} = \frac{\Delta z_{i+1} E_i^{n+1} + \Delta z_i E_{i+1}^{n+1}}{\Delta z_i + \Delta z_{i+1}}, \tag{64}$$

which is a weighted average of the cell center quantities. Using this value for the radiation energy density causes the piecewise linear variation in Eqs. (62) and (63) to be continuous from cell to cell. Substituting Eq. (64) into Eqs. (62) and (63) yields:

$$F_{l,i+1/2}^{n+1} = F_{r,i+1/2}^{n+1} = -\frac{2c}{3\kappa}\frac{(E_{i+1}^{n+1} - E_i^{n+1})}{\Delta z_i + \Delta z_{i+1}}, \tag{65}$$

which could have been written down intuitively, but then the implications of this equation would have not been clear. Inserting Eq. (65) into Eq. (61) produces a tridiagonal system of equations for the radiation energy density at time $n+1$:

$$-E_{i-1}^{n+1} + \left[1 + \frac{\Delta z_{i-1/2}}{\Delta z_{i+1/2}} + 3\kappa\Delta z_i \Delta z_{i-1/2}\gamma\left(1 + \frac{\kappa}{\gamma + \epsilon\kappa}\right)\right]E_i^{n+1} - \frac{\Delta z_{i-1/2}}{\Delta z_{i+1/2}} E_{i+1}^{n+1}$$

$$= 3\kappa\Delta z_i \Delta z_{i-1/2}\gamma E_i^n + \frac{3\kappa^2 \Delta z_i \Delta z_{i-1/2}\gamma}{\gamma + \epsilon\kappa}\theta_i^n, \tag{66}$$

where $\Delta z_{i+1/2} \equiv \frac{1}{2}(\Delta z_i + \Delta z_{i+1})$.

The application of the boundary condition takes several similar steps. First, one must recognize that $F(0, t) = F_{l,1/2}^{n+1}$ and that equating this value from Eq. (56) to Eq. (63) allows one to solve for the energy density at the surface:

$$E_{1/2}^{n+1} = \frac{\left(\frac{4}{c}F_{\text{inc}} + \frac{4}{3\kappa\Delta z_1}E_1^{n+1}\right)}{\left(1 + \frac{4}{3\kappa\Delta z_1}\right)}. \tag{67}$$

This can be substituted back into Eq. (63) to give $F_{r,1/2}^{n+1}$. Then Eq. (61) for the first cell becomes:

$$\left[1 + 2\left(\frac{\Delta z_1}{\Delta z_{3/2}} + \frac{4}{3\kappa\Delta z_{3/2}}\right)^{-1} + 3\kappa\Delta z_1 \Delta z_{3/2}\gamma\left(1 + \frac{\kappa}{\gamma + \epsilon\kappa}\right)\right]E_1^{n+1} - E_2^{n+1}$$

$$= 3\kappa\Delta z_1 \Delta z_{3/2}\gamma\left(E_1^n + \frac{\kappa}{\gamma + \epsilon\kappa}\theta_i^n\right) + \frac{8}{c}F_{\text{inc}}\left(\frac{\Delta z_1}{\Delta z_{3/2}} + \frac{4}{3\kappa\Delta z_{3/2}}\right)^{-1}. \tag{68}$$

At the other boundary, deep in the slab where the radiation has not yet reached, Eq. (4) sets $E_N^{n+1} = 0$. Alternatively, one could apply a zero flux boundary condition. After solving the system of equations for the radiation energy density, it is trivial to use Eq. (58) to evaluate the material energy density. In order to achieve a normalized solution that is comparable the analytic solution of the previous section, one must choose $4F_{\text{inc}}/c \equiv 1$. This will normalize the problem such that E and θ directly correspond to u and v.

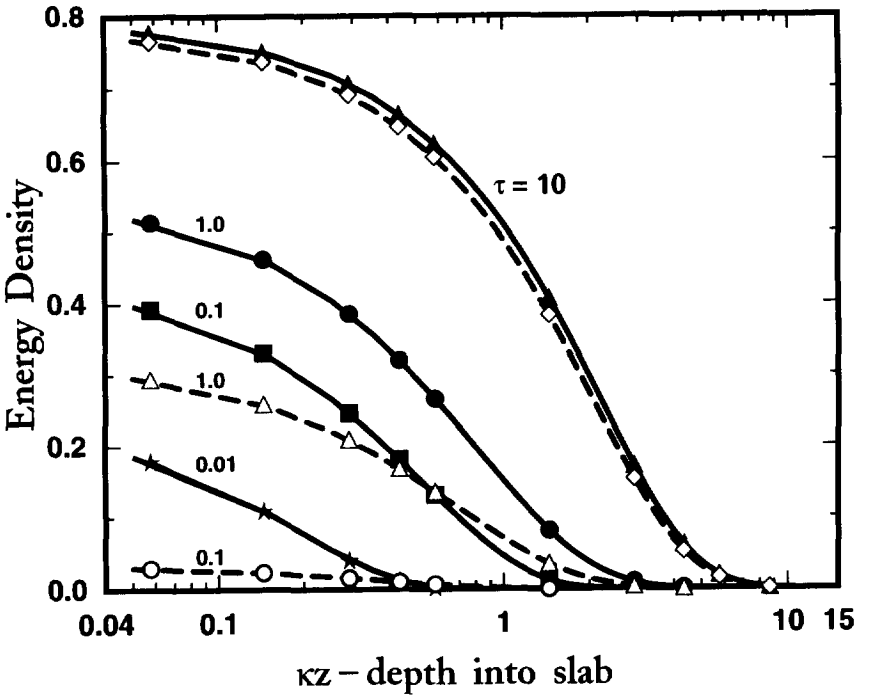

Fig. 2. Linear plot of the radiation energy density (——) and material energy density (---) as functions of position in the slab at different times. The symbols represent data from Tables 1 and 2.

After solving the system of equations [Eqs. (66) and (68)], it is normal procedure to refine the mesh and decrease the time step size until the solution appears to be converged. For this problem, with a uniform spatial mesh, convergence is apparently achieved with $\kappa\Delta z = 0.1$ and a time step chosen so that the maximum change in radiation energy density from one time step to the next is 5% in the zones with a non-zero radiation energy density. At the start of the solution, the time

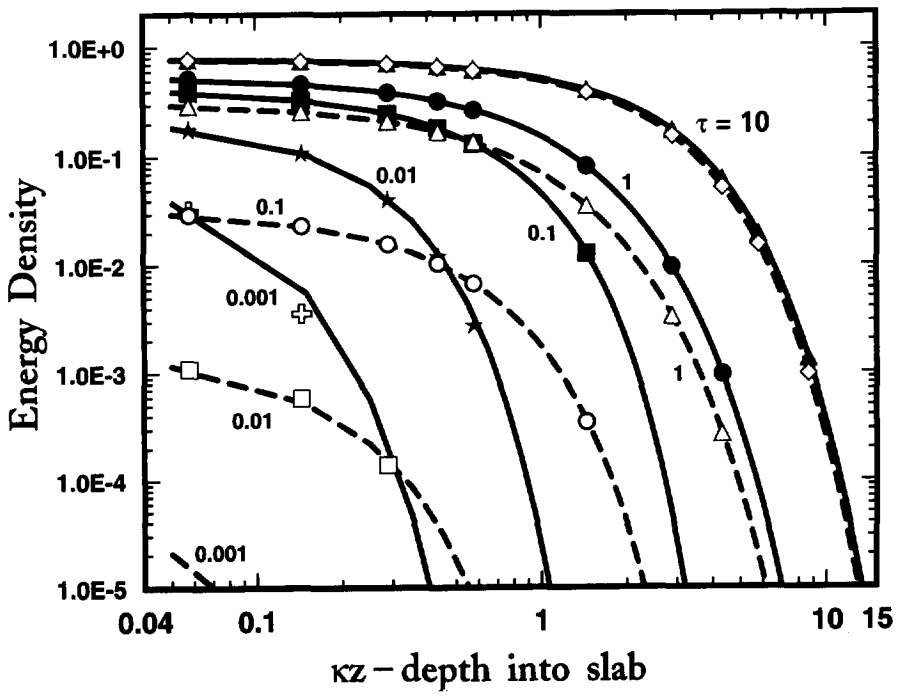

Fig. 3. Logarithmic plot of the radiation energy density (——) and material energy density (---) as functions of position in the slab at different times. The symbols represent data from Tables 1 and 2.

steps are $\Delta\tau \approx 1.0\,e-9$ (τ is the scaled time variable introduced in Sec. 2), and near $\tau = 10$ the time steps are $\Delta\tau \approx 0.03$. The solution for $\epsilon = 0.1$ is shown in Figs. 2 and 3. When plotted logarithmically, it is easier to see the early time behavior of the energy density. The linear plot shows the late time behavior to better advantage. These figures show that, as it should, the radiation penetrates into the slab quickly. The material energy density is slower to respond. At late times the two temperatures equilibrate and the physical problem becomes one of equilibrium diffusion.

The symbols shown in Figs. 2 and 3 represent the analytic point from Tables 1 and 2. Only the point for radiation energy density at $\tau = 0.001$ and $\kappa z = 0.15$ differs significantly from the numerical solution. In order to more accurately calculate this early time variation, a finer spatial mesh is required for the numerical solution. By decreasing the spatial mesh from 0.1 to 0.01, the error at this point drops from a factor of two to 1.5%. In the tables, only the points with values greater than 0.001 have enough significant digits to accurately compare to the numerical solutions. For these points at the times $\tau = 0.1$, 1, and 10, the mean deviation from the analytic points are 0.48, 0.39, an 0.19%, respectively, with a spatial mesh size of 0.1. Using the finer spatial mesh ($\kappa\Delta z = 0.01$), these mean deviations are 0.085, 0.072, and 0.14%.

Clearly, the analytic values from Tables 1 and 2 verify the accuracy of the numerical solution presented here. More importantly, this comparison validates the methods for generating the analytic benchmark and the finite difference solutions. Using completely different algorithms and arriving at the same solution strongy suggests that each solution has been done correctly. It is highly unlikely that either code has any remaining typographical, numerical, or logical errors. If such errors existed, one solution would not converge to the other solution.

5. CONCLUDING REMARKS

We have derived in this paper an analytic solution to the linearized non-equilibrium Marshak diffusion problem. Unlike the previous work,[3] we kept the speed of light as a finite constant in the equation of transfer in our treatment. The solution, in the form of finite integrals, was evaluated numerically by using Simpson's rule in each integration subrange. Typical numerical results were given for the distribution of the radiative energy and material temperature as a function of space and time. The analytic solution was compared with an asymptotic boundary layer solution and a finite difference solution, and very good agreements were achieved. This leaves no doubt that real benchmark results were obtained for the problem, because the solutions were generated in totally different ways. Since the integration convergence criteria used in computation is 0.001%, the maximum absolute error of the results is in the order of 10^{-5}. Therefore, the numerical results given in the tables are believed to be accurate up to at least the first four digits after the decimal point. In order to increase the number of significant digits of the small values (say less than 0.001) in the tables, one could attempt to do the calculations using a tighter convergence criteria. However, due to the strong oscillatory behavior of the integrands, the computation cost would be enormous, even if such a higher convergence criteria can be achieved practically by numerical methods.

The benchmark results for the non-equilibrium Marshak diffusion problem presented in this paper, along with the previously published results,[3] provide a rigorous benchmark test for validating time-dependent radiation diffusion computer codes. This is the true value of having the benchmark results.

Acknowledgements—This work was performed under the auspices of the U.S. Department of Energy. The authors are grateful to R. S. Baker for his valuable comments on the numerical scheme for evaluating the integrals.

REFERENCES

1. R. E. Marshak, *Phys. Fluids* **1**, 24 (1958).
2. W. Kass and M. O'Keeffe, *J. Appl. Phys.* **37**, 2377 (1966).
3. G. C. Pomraning, *JQSRT* **21**, 249 (1979).
4. G. C. Pomraning and I. R. Shokair, *JQSRT* **25**, 325 (1981).
5. B. D. Ganapol and G. C. Pomraning, *JQSRT* **29**, 311 (1983).
6. L. Råde and B. Westergren, *BETA—Mathematics Handbook*, Chap. 16.4, Studentlitteratur, Sweden (1992).
7. D. Mihalas and R. P. Weaver, *JQSRT* **28**, 213 (1982).